Pamukkale Üniversitesi Mühendislik Bilimleri Dergisi
Pamukkale University Journal of Engineering Sciences

Synthesis, DFT calculations, drug-likeness properties and molecular docking studies of a new oxime and its Ni(II) and Co(II) complexes.

Yeni oksim ve Ni(II), Co(II) komplekslerinin sentezi, DFT hesaplamaları, ilaç benzerlik özellikleri ve moleküler docking çalışmaları

Songül Anşin[1], Seda Alkan[1], Tufan Topal[2], Emin Karapınar[1]*

[1]Department of Chemistry, Faculty of Science, Pamukkale University, Denizli, Türkiye.
songulansin@gmail.com, sedaalkan1806@gmail.com, ekarapinar@pau.edu.tr
[2]Department of Chemical Engineering, Faculty of Engineering, Pamukkale University, Denizli, Türkiye.
ttopal@pau.edu.tr

Received/Geliş Tarihi: 03.06.2025 Revision/Düzeltme Tarihi: 07.07.2025 doi: 10.5505/pajes.2025.15729
Accepted/Kabul Tarihi: 14.07.2025 Research Article/Araştırma Makalesi

Abstract

In our study, the bidentate N-[(2E,3E)-3-{[(pyridin-4-yl)methyl]imino}butan-2-ylidene]hydroxylamine oxime ligand and its Ni(II) and Co(II) metal complexes were synthesized using a jacketed glass reactor, and structures were elucidated using some spectroscopic methods. LC/MS-MS and FT-IR spectra were investigated. The geometry of the optimized ligand was calculated by the DFT/B3LYP method at 6–31 G (d, p) levels. ^{13}C-NMR and ^{1}H-NMR chemical shift results, MEP maps, HOMO and LUMO gap energies, FT-IR spectra and geometric structure of the compound were characterized by the same method. It was shown that the experimental and theoretical calculations of ^{13}C-NMR, ^{1}H-NMR chemical shift results and FT-IR spectra were compatible with each other. Theoretical drug similarity studies were conducted for the synthesized molecules. Molecular docking studies have been used to elucidate the binding sites of molecules. The studies showed that the ligand molecule has high chemical stability.

Keywords: Oxime, Ni(II) and Co(II) complexes, Homonuclear complex, DFT

Özet

Çalışmamızda bidentat N-[(2E,3E)-3-{[(piridin-4-il)metil]imino}bütan-2-iliden]hidroksilamin oksim ligandı ve Ni(II) ve Co(II) metal kompleksleri ceketli cam reaktör kullanılarak belirlenen sıcaklıklarda sentezlendi ve yapıları bazı spektroskopik yöntemlerle aydınlatıldı. LC/MS-MS ve FT-IR spektrumları incelendi. Optimize edilmiş ligandın geometrisi 6–31 G (d, p) seviyelerinde DFT/B3LYP yöntemi ile hesaplandı. ^{13}C-NMR ve ^{1}H-NMR kimyasal kayma sonuçları, MEP haritaları, HOMO ve LUMO boşluk enerjileri, FT-IR spektrumları ve bileşiğin geometrik yapısı aynı yöntemle karakterize edildi. ^{13}C-NMR, ^{1}H-NMR kimyasal kayma sonuçları ve FT-IR spektrumlarının deneysel ve teorik hesaplamalarının birbiriyle uyumlu olduğu gösterildi. Sentezlenen moleküller için teorik ilaç benzerliği çalışmaları yapıldı. Moleküllerin bağlanma yerlerinin aydınlatılmasında moleküler kenetleme çalışmaları kullanıldı. Yapılan çalışmalar ligand molekülünün yüksek kimyasal kararlılığa sahip olduğunu göstermiştir.

Keywords: Oksim, Ni(II) ve Co(II) kompleksleri, Homonükleer kompleks, DFT

1 Introduction

Organic compounds featuring both pyridine and oxime groups have attracted significant attention from researchers due to their diverse applications across various fields, including medicine, agriculture, and industry. These compounds exhibit a remarkable range of biological activities, including antioxidant and anti-inflammatory properties, making them promising candidates for developing novel therapeutic agents.

Oximes, characterized by their versatility and reactivity, are valuable building blocks in organic synthesis. They act as precursors to amines and nitro compounds and play a critical role as intermediates in important reactions like the Beckmann rearrangement [1],[2]. Moreover, oximes are known for forming stable complexes with metal ions, leading to the development of various metal-based catalysts and materials [3],[4].

The pyridine ring, a common structural motif in many biologically active compounds, can enhance molecules pharmacological properties. Its presence often improves solubility, bioavailability, and target specificity [5]-[7]. When combined with the oxime functionality, the pyridine ring offers the potential to create compounds with unique properties and a wide range of applications. For instance, the presence of both pyridine and oxime groups in a molecule can lead to the formation of strong hydrogen bonds with biological targets, contributing to their enhanced biological activity.

Various synthetic methods have been employed to synthesize compounds containing both pyridine and oxime groups. These methods include condensation reactions, cyclizations, and metal-catalyzed coupling reactions [1],[8]-[10]. The choice of synthetic strategy is crucial and depends on factors such as the desired structure and complexity of the target molecule, the availability of starting materials, and the desired reaction yield and purity.

Research has demonstrated that organic compounds containing both pyridine and oxime groups exhibit excellent anti-inflammatory and antioxidant activity [1]. These compounds have shown strong binding energies and inhibition constants with cyclooxygenase enzymes (COX-2), suggesting their potential as anti-inflammatory agents [1],[10]. The anti-inflammatory effects of these compounds are attributed to their ability to inhibit the production of pro-inflammatory mediators, such as prostaglandins, which are involved in pain and inflammation.

*Corresponding author/Yazışılan Yazar

Additionally, these compounds demonstrate promising antioxidant activity, which is attributed to their ability to scavenge free radicals and prevent oxidative damage [1],[7]. Oxidative stress plays a role in various diseases, cardiovascular disease, including cancer and neurodegenerative disorders. Therefore, the development of effective antioxidants is of significant importance.

The combination of pyridine and oxime functionalities in a single molecule has opened up exciting avenues for the development of novel materials and catalysts. Researchers have explored the potential of these compounds as ligands for transition metal complexes, which have found applications in various catalytic processes, including Suzuki cross-coupling reactions.

The spectroscopic characterization of these compounds is crucial for understanding their structure, bonding, and electronic properties [1],[4],[8]. Techniques such as IR, NMR and UV-Vis spectroscopy are employed to elucidate the structural features and properties of these compounds.

Computational studies using density functional theory (DFT) calculations have also significantly contributed to understanding the electronic structure, reactivity, and properties of these compounds [1]. DFT calculations provide valuable insights into the molecular orbitals, energy levels, and electronic transitions, enabling researchers to predict and interpret experimental results.

In conclusion, organic compounds containing both pyridine and oxime groups represent a fascinating class of compounds with promising applications in various fields. Their unique properties, arising from the combination of these two functional groups, have led to the development of novel therapeutic agents, catalysts, and materials. Continued research in this area will undoubtedly yield further exciting discoveries and advancements, paving the way for new and innovative applications of these remarkable compounds.

Breast cancer is one of the most prevalent cancers among women worldwide, posing a significant threat to public health. Conventional treatments like chemotherapy often encounter challenges due to drug resistance and the potential for cancer recurrence. The quest for new molecules with enhanced efficacy in eradicating cancer cells remains an urgent priority. Oximes, with their unique chemical properties, have garnered increasing interest for their potential role in bolstering biological effects in drug development [11],[12]. Our study targets pharmaceutical agent compounds that will contribute to the treatment of breast cancer, one of the hormonal cancers, by using a type of protein called ER-α (Estrogen receptor alpha) [13].

Oxime groups, characterized by two H-bond acceptors (N and O) and one H-bond donor (OH), distinguish themselves from their carbonyl group counterparts. This distinction, along with their inherent polarity, may facilitate interactions with receptor binding sites, potentially leading to enhanced therapeutic effects. Moreover, the metabolic breakdown of oximes can release nitric oxide (NO). NO plays a crucial role in various physiological processes and has demonstrated anti-inflammatory and anticancer properties [14],[15].

Computational methods like molecular docking have revolutionized drug design by enabling the prediction of ligand-receptor interactions. These in silico approaches, coupled with DFT calculations, provide valuable insights into the binding mechanisms and molecular properties of potential drug candidates. The integration of spectroscopic data, DFT studies, and molecular docking analysis forms a powerful strategy for understanding the efficacy and selectivity of oxime compounds in targeting breast cancer. This holistic approach holds the promise of identifying novel therapeutic agents with improved potency and reduced side effects [16],[17].

In this study, the new ligand was synthesized by reacting diacetyl monoxime with pyridine. Subsequently, Ni(II) and Co(II) metal complexes of this ligand were successfully synthesized. A comprehensive suite of experimental methods including FT-IR, ^{1}H-NMR, ^{13}C-NMR, and LC/MS-MS were used for the characterization of the ligand and its complexes. In parallel, theoretical calculations including vibrational analysis, HOMO and LUMO energy determinations, geometric structure analysis, MEP analysis, and theoretical ^{13}C-NMR and ^{1}H-NMR calculations were performed to provide further insights and enable comparison with experimental data.

2 Materials and method

2.1 Material

The chemicals used during the study were supplied by companies named Fluka, Merck and Sigma Aldrich. Sodium metal, butyl nitrite, diethyl ether, ethanol, methanol, acetonitrile, acetophenone, acetic acid, pyridine amines, triethylamine (Et_3N), P_2O_5, $CaCl_2$ were used in our experiments. Ethyl alcohol was used during the crystallization processes, and acetonitrile and methanol were used in the synthesis process. NMR analyses were performed with a Bruker AVANCE III 400 MHz Model. FT-IR measurements were performed with a Perkin Elmer ATR-IR Spectrum Two Model instrument at 400-4000 cm^{-1}. Mass spectra were obtained with (ESI) TSQ Fortis™ Triple Quadrupole Mass Spectrometer. Melting points were measured with the Stuart SMP10 Model [18].

2.2 Synthesis of the N-[(2E,3E)-3-{[(pyridin-4-yl)methyl]imino}butan-2-ylidene]hydroxylamine oxime ligand

Diacetyl monoxime (10 mmol), 4-(Aminomethyl) pyridine (10 mmol) were dissolved in 10 mL of acetonitrile solvent and reacted with stoichiometric amounts (1:1) at room temperature using the classical method called condensation reaction. The reaction was terminated after continuing for 24 hours. The reaction was followed by a thin layer. After removing the solvent, the new oxime ligand was crystallized in ethyl alcohol. Then, it was dried over calcium chloride in a vacuum (Figure 1) [19]. Structures of the synthesized ligand were characterized by ^{1}H-NMR,^{13}C-NMR, FTIR and LC/MS-MS [20].

$C_{10}H_{13}N_3O$ Yield 82.6%. M.p.: 194–195 ˚C. FT-IR (cm^{-1}): 1004 (N-O), 1561 (C=N)$_{oxime}$, 1608 (C=N)$_{imine}$, 1625 (C=N)$_{pyridine}$, 2923 (C-H)$_{aliphatic}$, 3019 (C-H)$_{aromatic}$, 3265 (O-H). ^{1}H-NMR (400 MHz, Chloroform-d_6, ppm): δ 2.16 (s, 3H, -CH_3), δ 2.19 (s, 3H, -CH_3), δ 4.66 (d, 2H, Ar $_{pyridine}$ -H), δ 7.41 (d, 2H, Ar$_{pyridine}$ -H), δ 8.59 (s, 2H, aliphatic-H), δ 8.80 (s, 1H, O-H). ^{13}C NMR (100 MHz, Chloroform-d_6, ppm): δ 9.09 (-CH_3), δ 13.90 (-CH_3), δ 54.05 (C $_{aliphatic}$), δ 122.73, 122.73, 132.66, 149.55, 149.55 (C-Ar$_{pyridine}$), 158.87 (C=N$_{oxime}$), 165.90 (C=N$_{imine}$). LC/MS-MS Ms: (ESI) m/z= 191.22 $[M]^+$.

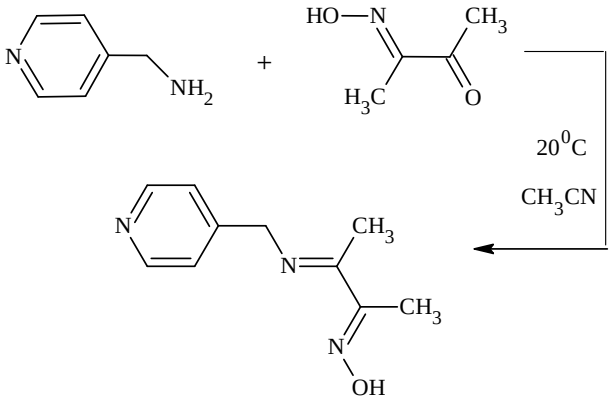

Figure 1. Synthesis of ligand.

2.3 Synthesis of the complexes

$Ni(NO_3)_2.6H_2O$ (0.290 g, 1 mmol), $Cu(NO_3)_2.3H_2O$ (0.241 g, 1 mmol) and $Co(NO_3)_2.6H_2O$ (0.290 g, 1 mmol) in 10 mL methanol solution were added separately to the ligand (0.382 g, 2 mmol) in 20 mL methanol solution. The resulting solution was boiled under reflux for 3 h and then cooled to 20 °C [21]. In addition, these complexes were verified by FTIR and LC/MS-MS [22]. The general representation of the synthesized $[L_2Ni]$ and $[L_2Co.2H_2O]$ compounds is shown in Figure 2a and 2b.

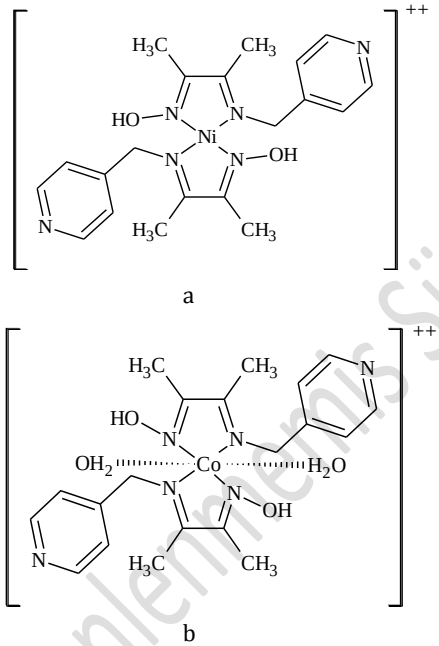

Figure 2. General representation of the synthesized complexes.

$[L_2Ni]$ $C_{20}H_{26}N_6NiO_2$ Yield 88.3%. M.p.: > 300 °C. FT-IR (cm^{-1}): 2922 $(C\text{-}H)_{aliphatic}$, 2993 $(C\text{-}H)_{aromatic}$, 3239 (O-H), 1551 $(C{=}N)_{oxime}$, 1615 $(C{=}N)_{imine}$, 1676 $(C{=}N)_{pyridine}$, 1024 (N-O), 484 (Ni–N). LC/MS-MS Ms: (ESI) m/z= 440.33 $[M\text{-}1]^+$.

$[L_2Co.2H_2O]$ $C_{20}H_{30}N_6CoO_4$ Yield 70.8%. M.p.: > 300 °C. FT-IR (cm^{-1}): 3242 (O-H), 3413 (H_2O), 3077 $(C\text{-}H)_{aromatic}$, 2922 $(C\text{-}H)_{aliphatic}$, 1563 $(C{=}N)_{oxime}$, 1614 $(C{=}N)_{imine}$, 1614 $(C{=}N)_{pyridine}$, 1007 (N-O), 482 (Co–N). LC/MS-MS Ms: (ESI) m/z= 478.17 $[M]^+$.

2.4 Calculation

In our study, the theoretical data of the synthesized ligand were calculated with the 6-31G(d,p) basis set using DFT/B3LYP. The theoretical and experimental data of the synthesized ligand were elucidated using Gaussian 09w and Gaussian View 6.0 package programs [23]. The vibration data obtained with VEDA4 (Vibrational Energy Distribution Analysis) Vibration Energy Distribution Analysis were obtained with Potential Energy Distribution (PED). The optimized molecular structure of the ligand by DFT/B3LYP/6-31G(d,p) method is shown in Figure 3. Also MEP analysis, HOMO and LUMO studies, NMR studies, geometric calculations were elucidated using this method [24]-[26].

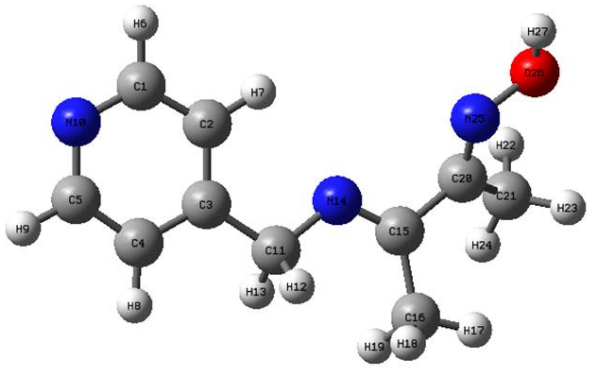

Figure 3. Optimized molecule.

3 Results and Discussion

3.1 Structural analysis

The optimization process was used to determine the most stable and lowest energy conformation of the ligand molecule. The structure was characterized by determining the bond lengths, bond angles and energies of the molecules. The characterized ligand consists of 27 atoms. It is seen that the structure has 43 bond angles, 27 bond lengths and 51 dihedral angles. The lengths for the optimized structure are C=N 1.2778 Å and O-H 0.9669 Å (Table 1).

3.2 NMR analysis

The experimental and theoretical ^1H and ^{13}C-NMR chemical shift values of the ligand molecule are in good agreement with the theoretical data. Experimental ^1H-NMR and ^{13}C-NMR spectrums of the ligand are shown in Figures 4 and Figure 5.

Table 1. Selected theoretical bond lengths, dihedral angles and bond angles of the ligand.

Atom	Bond length (Aº)	Atom	Bond angles (º)	Atom	Dihedral angles (º)
C1-C2	1.3959	C1-C2-C3	118.8182	C1-C2-C3-C4	0.0611
C3-C4	1.3993	C2-C1-H6	119.8099	C16-C15-C20-N25	-136.8919
C5-N10	1.3402	N25-O26-H27	101.9678	N25-C20-C21-H22	-52.0923
O26-H27	0.9669	H22-C21-H23	106.5223	C15-C20-C21-H24	7.4739
N25-O26	1.4040	C4-C3-C11	120.2668	C11-N14-C15-C20	-178.2862
N14-C15	1.2778				
C20-C21	1.5076				
C5-H9	1.0889				

When the ^{1}H NMR spectrum was examined, the experimental proton attached to the oxime group (–N=OH) was observed at 8.80 (1H) ppm and the theoretical proton at 7.17 ppm.

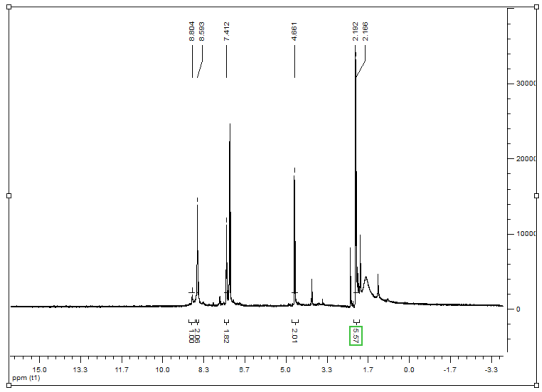

Figure 4. Experimental ^{1}H-NMR spectrum of the ligand.

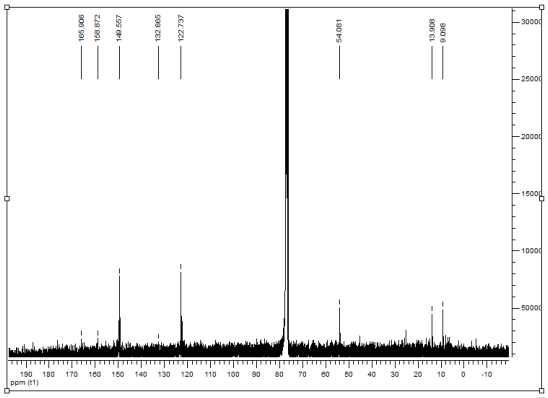

Figure 5. Experimental ^{13} C-NMR spectrum of the ligand.

The experimental single peak belonging to the –CH_2 protons acting as a bridge between 4-(Aminomethyl) pyridine and Diacetyl monoxime appeared at 4.66 (2H) ppm and the theoretical peaks at 4.64 and 4.65 ppm. The experimental protons attached to the pyridine ring appeared as a single peak at 8.59 ppm and the theoretical peaks 8.87 and 8.79 ppm and the other pyridine protons appeared as a single peak at 7.41 and the theoretical peaks 8.41 and 7.39 ppm. The title coumpound has a two methyl groups, experimental peaks belonging to the one methyl group (-CH_3) in the structure was observed at 2.19 ppm (3H) and the theoretical peaks 2.22, 2.07 and 2.01 and the other methyl group experimental peaks at 2.16 ppm (3H) and the theoretical peaks 2.46, 2.27 and 1.80 ppm [27]. Proton NMR of the structure is in good agreement with the literature data.

The experimental ^{13}C peaks of $(C=N)_{imine}$ and $(C=N)_{oxime}$ are 165.90 and 158.87 ppm, and the theoretical peaks are 154.26 and 146.37 ppm. Experimental peaks belonging to the aromatic pyridine ring are between 122.73-149.55 ppm and theoretical peaks are between 107.93-136.63 ppm. The experimental peaks of the methyl group were found as 13.90 and 9.09 ppm, while the theoretical peaks were found as 9.21 and 4.98 ppm. Calculated data and experimental values are given in Table 2. Correlation graphs of ^{1}H-NMR and ^{13}C-NMR's respectively y = 0.9845x + 0.0428 (R^2 = 0.9601) (Figure 6) and y = 0.9529x-4.5468 (R^2=0.9906) (Figure 7). Theoretical and experimental NMR results are in good agreement.

Table 2. Theoretical and experimental chemical shift data of the ligand.

Atom	Exp.	DFT	Atom	Exp.	DFT
H(27)	8.80	7.17	C(15)	165.90	154.26
H(6)	8.59	8.87	C(20)	158.87	146.37
H(9)	8.59	8.79	C(1)	149.55	135.62
H(7)	7.41	8.41	C(5)	149.55	134.32
H(8)	7.41	7.39	C(3)	132.66	136.63
H(12)	4.66	4.65	C(2)	122.73	108.75
H(13)	4.66	4.64	C(4)	122.73	107.93
H(17)	2.19	2.22	C(11)	54.08	44.74
H(18)	2.19	2.01	C(16)	13.90	9.21
H(19)	2.19	2.07	C(21)	9.09	4.98
H(22)	2.16	2.46			
H(23)	2.16	2.27			
H(24)	2.16	1.80			

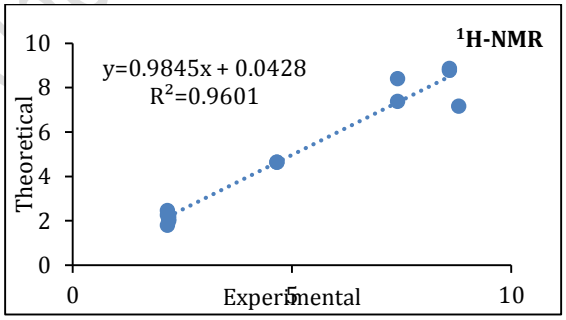

Figure 6. Correlation graph of calculated and experimental ^{1}H-NMR of the ligand.

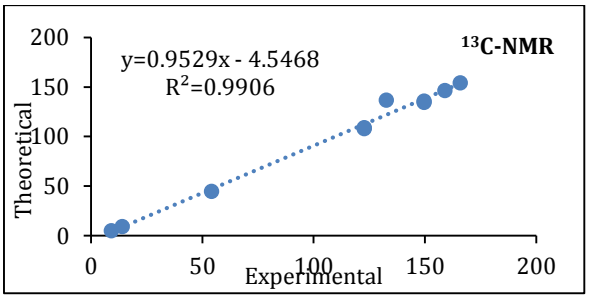

Figure 7. Correlation graph of calculated and experimental ^{13}C-NMR of the ligand.

3.3 FT-IR analysis

In our study, vibration modes were characterized in detail. The data were obtained using a correction factor of 0.9614. Theoretical and experimental data are in good agreement (Figure 8) [18].

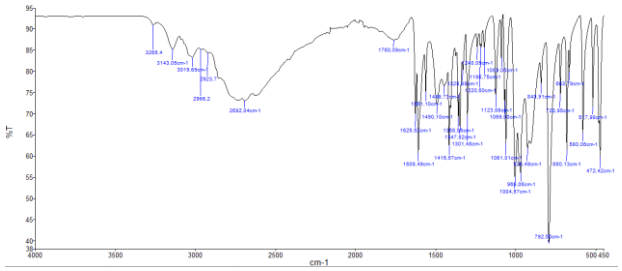

(a)

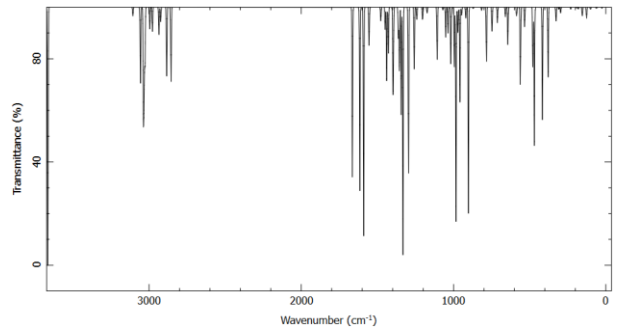

(b)

Figure 8. a) Experimental FT-IR, b) theoretical FT-IR spectra of the ligand compound.

In our study, a total of 140 vibration modes were found for the ligand, including 43 stretching, 48 bending, 44 torsion and 5 out. In general, 3 important IR absorbance bands were emphasized in the ligand compound, these are ν(O–H), ν(C=N) and ν(N–O) vibrations. Experimental $(C=N)_{oxime}$, $(C=N)_{pyridine}$, $(C=N)_{imine}$, vibration peaks of this ligand were observed at 1561 cm^{-1}, 1608 cm^{-1} and 1625 cm^{-1}, while theoretical vibrations were observed at 1590 cm^{-1}, 1615 cm^{-1} and 1664 cm^{-1} (Table 3). In addition, the O-H peak due to the oxime group appeared at 3664 cm^{-1} according to quantum calculations, while this peak appeared at 3265 cm^{-1} in experimental studies [28]. In experimental and theoretical studies, the peaks observed at 3019 cm^{-1} and 3026 cm^{-1} are attributed to the aromatic C-H peaks belonging to the pyridine ring [19],[29],[30]. Aliphatic C-H peaks were also observed at the same peak value (2923 cm^{-1}) in experimental and chemical calculation studies. Again, N-O peaks belonging to the oxime group were observed at 1004 cm^{-1} and 984 cm^{-1}. As a result, when the computer-based calculation program and experimental data of the compound were evaluated [31], it was seen that the results were very compatible with each other and the equality in the linear and correlation diagram was y=0.9464x + 56.276 (R^2 = 0. 0.9935) (Figure 9).

3.4 Analysis of complexes

The FTIR spectrum of complexes stretching vibrations at 1614 and 1676 cm^{-1}, 1614 and 1615 cm^{-1} for $[L_2Co.2H_2O]$ and $[L_2Ni]$ belong to $(C=N)_{pyridine}$ and $(C=N)_{imine}$. A shift in these bands was observed compared to the ligand. It was concluded that the (N-O) vibration bands of the complexes were 1007 and 1024 cm^{-1}. The (O-H) peaks that are decisive for oxime are 3242 and 3239 cm^{-1}. The peaks belonging to the (M-N) bond, which are not in the ligand but observed in the complexes, at 484 cm^{-1} for the $[L_2Ni]$ and 482 cm^{-1} for the $[L_2Co.2H_2O]$ (Figure 10-11).

Table 3. Selected vibrational assignments level of the ligand.

Scaled	IR Intensity	Assignments (%PED)
3665.93	85.68	ν OH(100)
3106.96	2.85	ν CH (98)
3057.38	25.16	ν CH (79)+ ν CH(20)
3038.51	31.56	ν CH(89)
2995.68	7.18	ν CH(-94)
2978.71	7.99	ν CH(-99)
2935.91	9.02	ν CH(77) + ν CH(-10)+ ν CH(10)
2924.85	4.76	ν CH(86)
2856.64	24.63	ν CH(97)
1665.31	56.34	ν NC (-77)
1615.88	60.88	ν NC (77)
1051.93	9.9	δ CCN (31) + δ HCN (23)+ δ HCN(12)
1037.13	8.55	τ HCCC (19)+ τ HCCC (-11) + ν ON(20)
967.63	1.39	τ HCNC(82)
958.285	31.45	τ HCCC(22) + ν ON(33)
643.667	12.35	δ CNO (62)
586.281	2.84	γ CCNC(54)

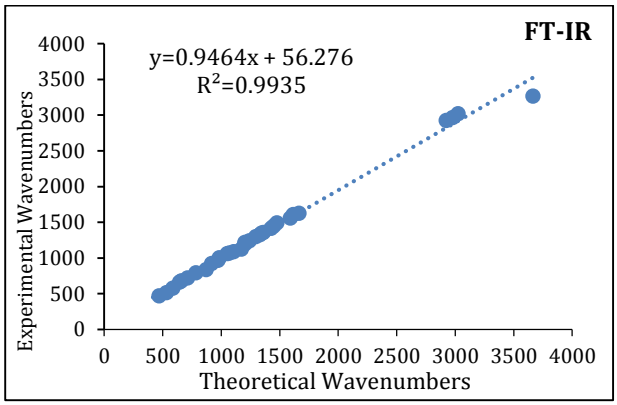

Figure 9. Correlation plot between experimental and calculated frequencies of the molecule ligand.

The mass spectrum results for the complexes were found to be (m/z, ESI) 440.33 $[M-1]^+$, 100% relative abundance and (m/z, ESI) 478.17 $[M+1]^+$, 10% relative abundance for $[L_2Ni]$ and $[L_2Co.2H_2O]$ respectively (Figures 12-13). For $[L_2Ni]$ complex other fragmentation peaks were seen at (m/z, ESI) 424.14, 382.06, 215.84 and 229.87 with abundances of 6%, 19%, 62% and 25%. The complex is square planar in structure. For $[L_2Co.2H_2O]$ other fragmentation peaks were seen at (m/z, ESI) 441.39, 424.38, 351.27, 340.28 and 274.18 with abundances of 10%, 80%, 18%, 10%, 100% and 95%. According to mass spectroscopy results, two water molecules were observed at (m/z, ESI) 478.17 (10%) [19]. Experimental results are by the structures suggested for the complexes. The complex has an octahedral structure. Mass spectra data and fragmentation products of the complexes are shown in Table 4.

Table 4. Mass spectra data and fragmentation products of the complexes.

Molecule	m/e	Relative abundance (%)	Fragment
	440.33	100	$[M-1]^+ C_{20}H_{26}N_6NiO_2$
$[L_2Ni]$	424.14	6	$[M+1]^+ C_{20}H_{25}N_6NiO$
$C_{20}H_{26}N_6NiO_2$	382.06	19	$[M+1]^+ C_{17}H_{19}N_6NiO$
	215.84	62	$[M+2]^+ C_5H_9N_4NiO_2$
	229.87	25	$[M-2]^+ C_6H_{11}N_4NiO_2$
	478.17	10	$[M+1]^+ C_{20}H_{30}N_6CoO_4$
	441.39	80	$[M+1]^+ C_{20}H_{26}N_6CoO_2$
$[L_2Co.2H_2O]$	424.38	18	$[M-5]^+ C_{20}H_{25}N_6CoO$
$C_{20}H_{30}N_6CoO_4$	351.27	10	$[M-2]^+ C_{16}H_{16}N_6Co$
	340.28	100	$[M+2]^+ C_{16}H_{19}N_5Co$
	274.18	95	$[M]^+ C_{11}H_{13}N_5Co$

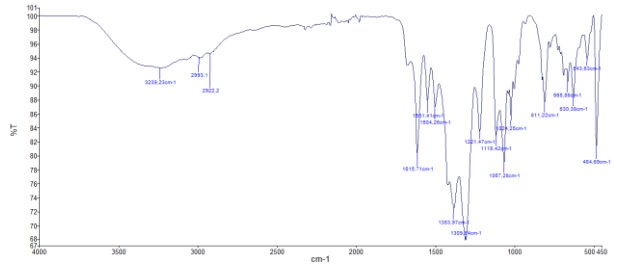

Figure 10. FT-IR spectrum of $[L_2Ni]$.

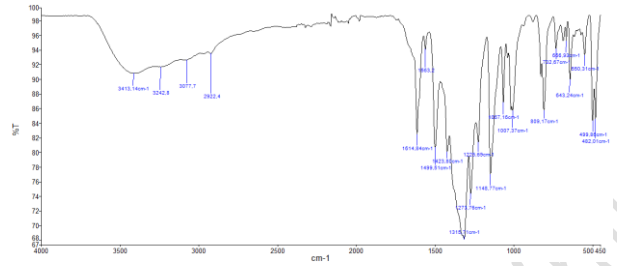

Figure 11. FT-IR spectrum of $[L_2Co.2H_2O]$.

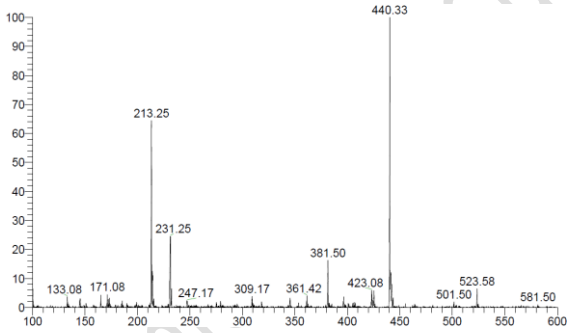

Figure. 12. LC-MS/MS Spectrum of $[L_2Ni]$.

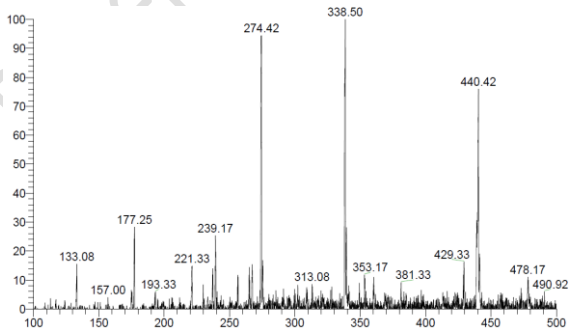

Figure 13. LC-MS/MS spectrum of $[L_2Co.2H_2O]$.

3.5 HOMO-LUMO studies

The energy difference between LUMO and HOMO having energy levels in the molecule makes an important contribution to the determination of spectroscopic properties, stability, chemical properties, chemical reactivity and electronic transitions of the structure in the molecule. The HOMO-LUMO energy orbitals examined are shown in Figure 14. The green colored parts show negative areas and the red colored parts show positive areas. E_{LUMO} -1.0966 eV, E_{HOMO} -6.5851 eV, E_{LUMO+1} -0.3319 eV, E_{HOMO-1} -6.3810 eV were found. When the calculations are examined, the energy values between LUMO-HOMO and LUMO+1-HOMO-1 for the ligand were 5.4885 eV and 6.0491 eV. This showed that the structure has low chemical reactivity and high kinetic stability. The parameters that determine the reactivity and stability of the structure are chemical hardness and chemical softness 2.7442 and 0.1822; electronegativity 3.8408; chemical potential -3.8408; ionization potential 6.5851 and electron affinity 1.0966 [18], [32],[33].

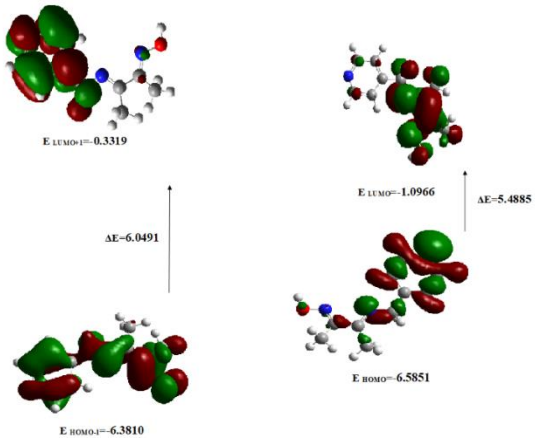

Figure 14. HOMO-LUMO orbitals of the ligand.

3.6 MEP Analysis

The charge distribution in the molecule gives the molecular electrostatic potential. In the map, red areas represent electrophilic attack and negative sites, while blue areas represent positive sites and nucleophilic attack sites. Also, the blue color represents attraction, and the red color represents repulsion. MEP results of the ligand were found as -5.848 e^{-2} and 5.848 e^{-2} (Figure 15). Negative sites were found on the hydrazone and nitrogen atom. 2D map proves proton transfer [19],[32]-[34].

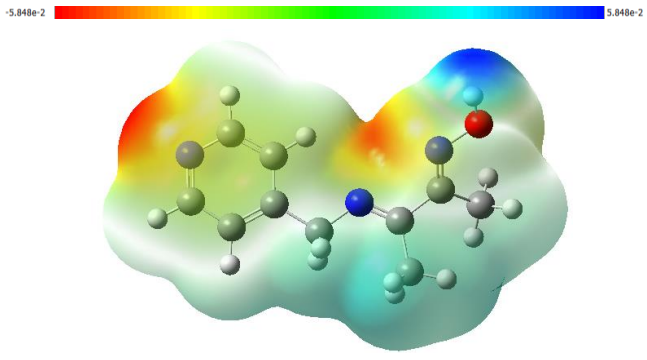

a)

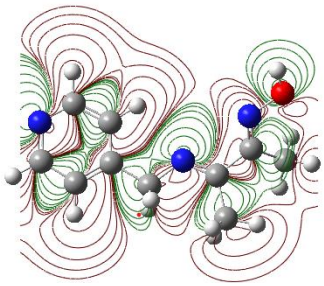

b)

Figure 15. a) 3D map and b) 2D contour map for ligand.

3.7 Drug-Likeness of ligand and complexes

Lipinski's five rules, which allow the preparation and design of drugs and predict properties such as clogP, the number of hydrogen bond donors and acceptors, molecular weight are as follows:

1. Number of hydrogen bond acceptors ≤10
2. Molecular weight (MW) ≤500 Da
3. Capacity to pass through the cell membrane miLogP ≤5
4. Number of hydrogen bond donors ≤5
5. Polar surface area of the molecule (TPSA) ≤140

The drug similarity of ligands and complexes was determined with the application of Molinspiration (http://www.molinspiration.com/) [35],[36]. The molecular weight is less than the limit value for all molecules. Having a small molecular weight is an important criterion for the drug to pass into the bloodstream, into the intercellular space and be excreted from the body. The cell membrane permeation capacity, which should be less than 5, is below this value for all three molecules. The donor hydrogen bond number is nOHNH ≤ 5 and the results are below this value except for [$L_2Co.2H_2O$]. The hydrogen bond potential is suitable for the molecules. The hydrogen bond number of nON ≤ 10 is suitable for this value [31]. The drug similarity values calculated for the three molecules are shown in Table 6. It was determined that the [L_2Ni] complex showed better drug similarity than the [$L_2Co.2H_2O$] complex.

Table 5. Calculated drug-likeness parameters of complexes and ligand.

	Ligand	[L_2Ni]	[$L_2Co.2H_2O$]
miLogP	0.73	-6.51	-6.79
TPSA	57.85	78.26	125.02
natoms	14	29	31
MW	191.23	441.16	477.43
nON	4	8	10
nOHNH	1	2	6
nviolations	0	0	1
nrotb	3	4	4

3.8 Molecular docking

The best way to examine the interactions between ligand and protein is molecular docking studies. This technique has been frequently used in recent years to elucidate drug-target protein interactions by providing the best simulation. Thanks to the Autodock vina algorithm, the interaction with the lowest binding energy and the most hydrogen bonds was taken as the basis for determining the position between the ligand and protein [37]. Hydrogen bonding and other interactions of the compounds with the 1U3G (Figure 16) protein were performed using Biovia Discovery Studio (DS) visualizer [38].

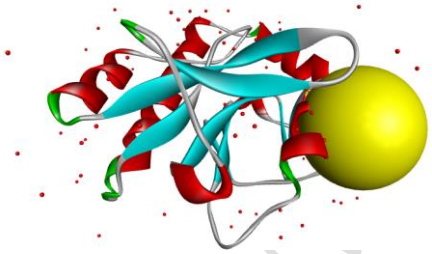

Figure 16. Main protease (1U3G) of breast cancer

The parameters were kept at their default settings and a 30 x 30 x 30 grid box was taken. The size of the grid box X= 0.90, Y=19.47, Z=24.82. The binding affinity of the ligand to the 1U3G protein was determined as -6.7 and it exhibited four types of interactions. Hydrogen bonding between the ligand and amino acid residue GLU55, Pi-cation with ARG115, Pi-Pi T-Shaped with TYR122, Pi-alkyl interactions with LYS120 were observed [13]. When the interactions were evaluated in general, two hydrophobic, one electrostatic and one hydrogen bond interactions were shown in Figure 17. Seven interactions were observed between the nickel complex and breast cancer protease. These were determined as two conventional hydrogen bonds with MET1 and ASP2, two hydrogen bonds with ASP151:O1 and ASP151:O2, one pi-sigma and two pi-alkyl (Figure 18). Pi-sigma and Pi-alkyl bonds in the hydrophobic category also have low binding energy [18]. The binding affinity of the Ni complex was found to be -7.9. Six types of interactions

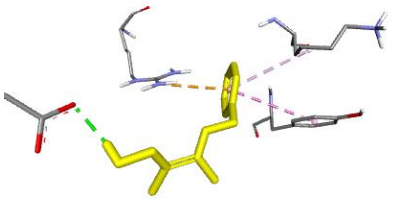

a)

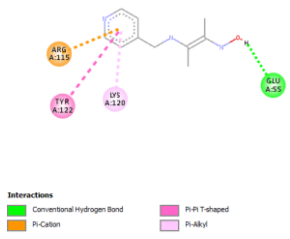

b)

Figure 17. a) Ligand interaction with the active site of 1U3G b) 2D structure of ligand-receptor interaction.

were observed between the Co complex and 1U3G amino acid residues. One conventional hydrogen bond interacted with LEU127, two hydrogen bonds with ASP154 and GLN156, one Pi-Anion bond with ASP158, one Pi-Sulfur bond with MET128,

and one Pi-alkyl bond with VAL155 residues. The binding affinity of the Co complex against breast cancer was found to be 7.4. When the inhibitor-receptor interactions of the compounds were evaluated in general terms, the highest binding affinity was observed in the Ni complex, revealing that this compound, with the strongest binding, has the best inhibitory capacity [39],[40]. This is consistent with the theoretical drug similarity studies.

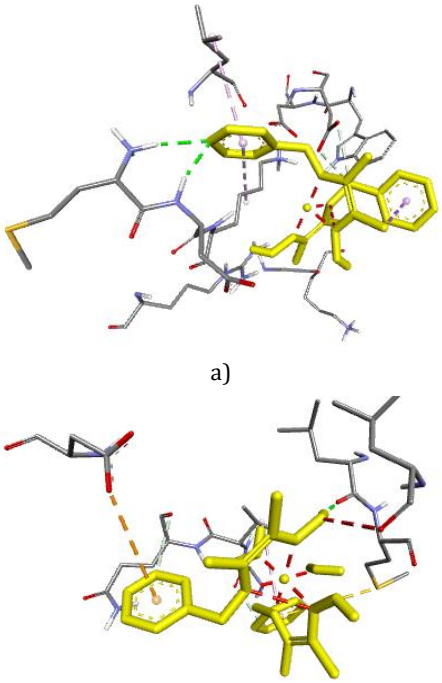

a)

b)

Figure 18. Complexes interaction with the active site of 1U3G **a)** [L_2Ni] **b)** [$L_2Co.2H_2O$].

4 Conclusion

N-[(2E,3E)-3-{[(pyridin-4-yl)methyl]imino}butan-2-ylidene] hydroxylamine oxime was synthesized and characterized by spectroscopic methods. Experimental data are in agreement with the literature. DFT calculations were performed for the ligand molecule, ^{13}C-NMR and ^{1}H-NMR, FT-IR, HOMO-LUMO analysis, geometric parameters and MEP mapping studies were performed. It was seen that the theoretical results of NMR and vibrational analysis studies were consistent with the experimental results. The HOMO-LUMO difference was found to be 5.4885 eV. Molecular electrostatic potential was mapped to identify electrostatic fields and nucleophilic reactions. Studies have shown that the ligand molecule has high chemical stability. As a result of the theoretically calculated drug similarity study, more compatible results were obtained for the ligand and [L_2Ni] complex. As a result of molecular docking studies, the binding affinities of the ligand, Ni complex and Co complex are -6.7, -7.9 and -7.4 kcal/mol, respectively. It was seen that the [L_2Ni] complex had better docking compared to the ligand and [$L_2Co.2H_2O$] complex.

5 Acknowledgements

This work was supported by Research Fund of the Pamukkale University (Project Number: 2021FEBE033).

6 Author contribution statements

In the study carried out, Author 1 did the experimental work, writing; Author 2 designed, theoretical calculation studies, writing; Author 3 theoretical calculation studies, writing and Author 4 methodology, supervised the project spectroscopic analysis and edited the manuscript.

7 Ethics committee approval and conflict of interest statement

"There is no need to obtain permission from the ethics committee for the article prepared". "There is no conflict of interest with any person/institution in the article prepared".

8 References

[1] Bozbey I, Uslu H, Türkmenoğlu B, Özdemir Z, Karakurt A, Levent S. "Conventional and microwave prompted synthesis of aryl(alkyl)azole oximes, 1H-NMR spectroscopic determination of E/Z isomer ratio and HOMO–LUMO analysis". Journal of Molecular Structure, 1251, 132077, 2022.

[2] Çelik C, Ulukanlı Z, Tümer M, Serin S. "Spectroscopic characterization of oxime ligands and their complexes". Spectrosc. Lett., 36, (1-2), 51-70, 2003.

[3] Dinda S, Ghosh S, Pramanik K, Ganguly S. "An unusual coordination behavior of an oxime of 2-acetylnaphthalene in cobalt(III) complex: Structural and theoretical studies". Journal of Molecular Structure, 1241, 130635, 2021.

[4] Hong S, Chen G, Wu J, Zhu X. "Nickel-catalyzed asymmetric reductive cyclization of cyclohexadienones with O-benzoyloximes". Nature Communications, 11(1), 5170, 2020.

[5] Kaya Y, Yilmaz V T, Arslan T, Buyukgungor O. "Experimental and theoretical DFT studies of structure, spectroscopic and fluorescence properties of a new imine oxime derivative". Journal of Molecular. Structure, 1024, p. 65-72, 2012.

[6] Serbest K, Dural T, Emirik M, Zengin A, Faiz Ö. "Heteroligand bivalent transition metal complexes with an azo-oxime ligand and 1,10-phenanthroline: Synthesis, spectroscopy, thermal analysis, DFT calculations and SOD-mimetic activities". Journal of Molecular. Structure, 1229, 129579, 2021.

[7] Shiralini A, Samiee S, Hoveizi E. "Synthesis and characterization of mononuclear oxime-based palladacycles incorporating phosphorus ylides application as a catalyst in Suzuki cross cou". Journal of Coordination Chemistry, 74(15), 2542–2557, 2021.

[8] Sumathi T, Nithya R, Kamatchi S. "Synthesis, theoretical investigation, antioxidant and anti-inflammatory activity of di-tert-butyl (E)-4-hydroxy-6-(hydroxyimino)-4-methyl-2-arylcyclohexane-1,3-dicarboxylate derivatives: A combined experimental and computational approach". Chemical Physics Impact, 8, 100583, 2024.

[9] Yan L, Dong W. "Synthesis, crystal structures and spectroscopic properties of two Cu(II) complexes containing oxime ligands, Journal of Structural Chemistry". Journal of Structural Chemistry, 52(5), 1043-1049, 2011.

[10] Zhao L, Duan J, Tian F. "Synthesis and spectral characterization of oxime ligands and their Ni(II), Cu(II) complexes and their catalytic activity of Henry reaction". Spectrochimica Acta Part A: Molecular and Biomolecular Spectroscpy, 248, 119206, 2011.

[11] Shtaiwi A, Adnan R, Khairuddean M, Kha, S U. "Computational investigations of the binding mechanism of novel benzophenone imine inhibitors for the treatment of breast cancer". The Royal Society of Chemistry, 9, 35401-35416, 2019.

[12] Canário C, Matias M, Brito V A, Santos O, Falcão A, Silvestre S, Alves G. "New Estrone Oxime Derivatives: Synthesis, Cytotoxic Evaluation and Docking". Molecules, 26, 2687, 2021.

[13] Ragavana I, Vidyaa C, Shanavasa S, Acevedob R, Anbarasana P M, Manjric A, Prakasamd A, Sudhakare C, Selvankumare T, "Synthesis, spectroscopic characterization and molecular docking study of ethyl 2-(4-(5, 9-dihydro-6-hydroxy-2-mercapto-4H-purin-8-ylthio) thiophen-2-yl)-2-oxoacetate molecule for the chemotherapeutic treatment of breast cancer cells". Chemical Physics, 530, 110596, 2020.

[14] Schepetkin I A, Plotnikov M B, Khlebnikov A I, Plotnikova T M, Quinn M T. "Oximes: Novel Therapeutics with Anticancer and Anti-Inflammatory Potential". Biomolecules, 11, 777, 2021.

[15] Kosmalski T, Hetmann A, Studzinska R, Baumgart S, Kupczyk D, Roszek K. "The Oxime Ethers with Heterocyclic, Alicyclic and Aromatic Moiety as Potential Anti-Cancer Agents". Molecules, 27, 1374, 2022.

[16] Ayub Md A, Tyagi A R, Srivastava S K, Singh P. "Quantum DFT analysis and molecular docking investigation of various potential breast cancer drugs". Royal Society of Chemistry, 13, 218-238, 2025.

[17] Semire B, Oyebamiji A K. "Theoretıcal Studıes on Pyrazole Derıvatıves as Antıbreast Cancer Agents: DFT, QSAR and Dockıng Methods". Bulletin of Pharmaceutical Research, 7(3), 150, 2017.

[18] Topal T, Zorlu Y, Karapınar N. "Synthesis, X-ray crystal structure, IR and Raman spectroscopic analysis, quantum chemical computational and molecular docking studies on hydrazone-pyridine compound: as an insight into the inhibitor capacity of main protease of SARS-CoV2". Journal of Molecular. Structure, 1239, 130514, 2021.

[19] Topal T. "Spectroscopic and quantum chemical studies on the structure of 3-chloro-2-{(2Z)-2-[1-(4-methoxyphenyl)ethylidene]hydrazinyl}pyridine". Gazi University, 35(2), 404-419, 2022.

[20] İlkimen H, Gülbandılar A. "Synthesis, characterization, anti-microbial activity studies of 2-methoxy-5-sulfamoylbenzoic acid and 2-aminopyridine derivatives salts and their Cu(II) complexes". Pamukkale University Journal of Engineering Sciences, 30(7), 1009-1018, 2024.

[21] Topal T. "Synthesis, X-ray, characterization and HSA and energy framework analysis of novel pyridinehydrazone based ligand and its Co(II) complex biological activity prediction and experimental antibacterial properties". Molecular Crystals and Liquid Crystals, 741(1), 94-113, 2022.

[22] İlkimen H. "A review on biological properties and mixed ligand metal complexes of 2-aminobenzothiazole". Pamukkale University Journal of Engineering Sciences, 24(7), 1360-1369, 2018.

[23] Parlak C, Alver Ö. "Carbonyl stretching vibrations of 5-halogen-2-thiophenecarboxaldehydes: KBM, AN, SWAIN and LSER parameters". Pamukkale University Journal of Engineering Sciences, 22(7), 609-612, 2016.

[24] Frisch M J, et al., G16_B01. Gaussian 16, Revision B.01. Gaussian, Inc., Wallingford CT, 2016.

[25] Bilge D. "Conformational and FTIR analyses of 2,3-dimethoxyphenylboronic acid". Pamukkale University Journal of Engineering Sciences, 25(7), 899-903, 2019.

[26] Sert Y. "Vibrational, geometrical and HOMO/LUMO/MEP analyses by using DFT/B3LYP and DFT/M06-2X methods: 3-Amino-1,2,4-triazole". Pamukkale University Journal of Engineering Sciences, 24(7), 1272-1277, 2018.

[27] Karapinar E, Karapinar N, Ozcan E, Coskun A. "Synthesis, Characterization and Extraction Properties of Four Unsymmetricall vic-Dioximes and their Complexes with Nickel (II), Cobalt (II) and Copper (II), Synthesis and Reactivity in Inorganic". Metal-Organic and Nano-Metal Chemistry, 37(8), 611-619, 2007.

[28] Topal T. "Synthesis and characterization of zinc(II) complexes with new pyridine-based ligands: crystal structure, Hirshfeld surface analysis, and molecular docking study of lung cancer cell". Journal of Coordination Chemistry, 7323(23), 3203-3222, 2020.

[29] Karapinar E, Karapinar N, Ozcan E. "Synthesis of N′-(4′-Benzo[15-crown-5] phenylaminoglyoxime and Its Complexes with Copper(II), Nickel(II), and Cobalt(II), Synthesis and Reactivity in Inorganic". Metal-Organic and Nano-Metal Chemistry, 33(8), 1319, 2003.

[30] Karapinar E. "Synthesis and Characterization of a New (E,E)-Dioxime and its Homonuclear Complexes". Journal of Inclusion Phenomena and Macrocyclic Chemistry, 53, 171-175, 2005.

[31] Topal T. "Synthesis, Crystallographic Structure, Hirshfeld Surface Analysis, Drug-likeness Properties and Molecular Docking Studies of New Oxime-pyridine Compounds". Acta Chim. Slov., 68, 88-101, 2021.

[32] Alkan S, Topal T, Karapinar E. "Synthesis and Characterization of New Oxime Ligand and Its Cu(II)

Complex: DFT Calculations, in Vitro Antibacterial Activity, Drug-Likeness Properties, and Molecular Docking Studies". Russian Journal of Physical Chemistry A, 98(5), 1065-1075, 2024.

[33] Dede B, Aysan O, Yildirim F. "Synthesis, Spectroscopic Properties, and DFT Calculations of Novel Naphthoquinone Based Diimine Molecule". Russian Journal of Physical Chemistry A, vol. 95(1), 99-108, 2021.

[34] Korkmaz U, Fındık B T, Dede B, Karipcin F. "Synthesis, structural elucidation, in vitro antibacterial activity, DFT calculations, and molecular docking aspects of mixed-ligand complexes of a novel oxime and phenylalanine". Bioorg. Chem., 121, 105685, 2022.

[35] Lipinski C A, Lombardo F, Dominy B W, Feeney P J. Adv. Drug Deliv. Rev., 46, 3-26, 2001.

[36] Lipinski, C A. Drug Discov. Today. Technol., 1, 337-341, 2004.

[37] Trott O, Olson A J. "AutoDock Vina: Improving the speed and accuracy of docking with a new scoring function, efficient optimization, and multithreading". J. Comput. Chem., 31(2), 455-461, 2009.

[38] Dassault Systemes BIOVIA, Discovery Studio Modeling Environment, Release, San Diego: Dassault Systemes, 2017.

[39] Gatfaoui S, Sagaama A, Issaoui N, Roisnel, T, Marouani H. "Synthesis, experimental, theoretical study and molecular docking of 1-ethylpiperazine-1,4-diium bis(nitrate)". Solid State Sci., 106, 106326, 2020.

[40] Göktürk, T., Zengin, T., Hökelek, T., Gokce, C., and Gup, R., "Synthesis, Crystal Structure, Hirshfeld Surface Analysis, DNA/BSA Interaction and Molecular Docking Studies of 2-(6-(4-chlorophenyl)-1,2,4-triazin-3-yl)quinoline". Journal of Molecular Structure, 1292, 136128, 2023.